J. Phys. B: Atom. Molec. Phys., Vol. 9, No. 14, 1976. Printed in Great Britain.

Differential and integral cross sections for proton–hydrogen scattering

R Schinke† and H Krüger

Fachbereich Physik, Universität Kaiserslautern, 675 Kaiserslautern, Federal Republic of Germany

Received 21 January 1976, in final form 15 April 1976

Abstract. Elastic and inelastic, direct and exchange differential cross sections have been calculated for proton–hydrogen scattering in the energy range 250 eV $\leqslant E_{lab} \leqslant$ 2000 eV. The results are compared with recent experimental data and with other theoretical predictions. We applied the impact-parameter approximation and expanded the electronic wavefunction into adiabatic electronic states. Both straight-line and Coulomb trajectories have been used to integrate the set of coupled equations. Furthermore the influence of the size of different molecular bases on the cross sections is studied and qualitatively explained in terms of the rotational couplings between the various Σ and Π states. Finally, integral cross sections for the $2p_{\pm 1}$, 2s, $2p_0$ and $3p_{\pm 1}$ excitation are calculated in the range of 1 keV $\leqslant E_{lab} \leqslant$ 10 keV.

1. Introduction

Recent measurements of the differential cross sections for elastic, charge-exchange and $2p_{\pm 1}$ excitation processes in proton–hydrogen scattering (Houver *et al* 1974) indicate that the straight-line eikonal approximation (McCarroll and Piacentini 1970, Chidichimo-Frank and Piacentini 1974) gives excellent results for small scattering angles, while it may be subject to errors at larger angles. Gaussorgues *et al* (1975) took proper account of the internuclear Coulomb repulsion, which dominates the scattering at larger angles. Their 'common trajectory' method gives results which agree very well with the measured cross sections even for larger angles. It is therefore of interest to investigate the influence of choosing more realistic trajectories within this impact-parameter approximation.

Bates and Williams (1964) showed that the major non-adiabatic effect in low-energy proton–hydrogen scattering is due to the $2p\sigma_u \rightarrow 2p\pi_u$ rotational coupling at small internuclear separations. Rosenthal (1971) and Chidichimo-Frank and Piacentini (1974) enlarged the molecular expansion basis by including also the $3p\sigma_u$ and $3p\pi_u$ states which give rise to $2p_0$, 2s and $3p_{\pm 1}$ excitations. They found that the inclusion of these states changes the elastic, total charge-exchange and $2p_{\pm 1}$ excitation cross sections only very slightly. But this may not be true for the excitation of the 2s, $2p_0$ and $3p_{\pm 1}$ states, which takes place by two-step coupling. Recently non-adiabatic coupling elements have been reported not only for ungerade but also

† Work performed in partial fulfilment of the requirements for the PhD degree, Fachbereich Physik, Universität Kaiserslautern, Federal Republic of Germany.

for gerade states by Schinke and Krüger (1976) and Hatton *et al* (1975). Therefore it is of interest to present cross section calculations which also include the corresponding gerade states. The resulting cross sections can be interpreted qualitatively in terms of the united-atom limit of the angular-momentum matrix elements $\langle\alpha|iL_y|\beta\rangle$.

In §2 we present the basic formulae for calculating differential and integral cross sections within the adiabatic impact-parameter approximation. The results obtained by using both several expansion sets and different trajectories are presented and discussed in §3. Atomic units have been used throughout except where otherwise stated.

2. Theory

Adopting the impact-parameter approximation, one assumes that the relative motion of the two nuclei proceeds along classical trajectories $\boldsymbol{R} = \boldsymbol{R}(t)$, determined by a potential whose choice is usually guided by rather rough physical arguments. In this work we choose straight lines ($V = 0$) and Coulomb trajectories ($V = 1/R$). Then for the motion of the electron in the field of the two protons one determines the electronic wavefunction $\psi(\boldsymbol{r}, \boldsymbol{R}(t))$ as a solution of the time-dependent Schrödinger equation. To do this, we expand ψ into the adiabatic wavefunctions $\psi_i^{g(u)}(\boldsymbol{r}, R)$ with energies $\epsilon_i^{g(u)}(R)$ according to

$$\psi(\boldsymbol{r}, t) = \frac{1}{\sqrt{2}} \sum_j [a_j^+(\psi_j^g + \psi_j^u) + a_j^-(\psi_j^g - \psi_j^u)] \exp\left(-\frac{i}{2}\int_{-\infty}^{t} dt(\epsilon_j^g + \epsilon_j^u)\right) \tag{1}$$

where the superscripts g and u distinguish gerade and ungerade wavefunctions. Both $\psi^{g(u)}$ and $\epsilon^{g(u)}$ become time-dependent through the trajectory $\boldsymbol{R}(t)$. After insertion of (1) into the time-dependent Schrödinger equation the coefficients $a_j^{+(-)}$ are seen to satisfy the following set of coupled equations:

$$\dot{a}_j^{+(-)} = -\frac{1}{2}\left[\sum_{i\neq j}[A_{ji}^g(a_i^+ + a_i^-)_{(+)}A_{ji}^u(a_i^+ - a_i^-)] \times \exp\left(-\frac{i}{2}\int_{-\infty}^{t}(\epsilon_i^g - \epsilon_j^g + \epsilon_i^u - \epsilon_j^u)\right) + i(\epsilon_j^g - \epsilon_j^u)a_j^{-(+)}\right]. \tag{2}$$

The non-adiabatic coupling matrices $\mathbf{A}^{g(u)}$ are real and antisymmetric and their elements can be split into radial and rotational contributions (Rosenthal 1971) according to

$$A_{ji}^{g(u)} = \frac{dR}{dt}\left(\psi_j^{g(u)}, \frac{d}{dR}\psi_i^{g(u)}\right) + \frac{vb}{R^2}(\psi_j^{g(u)}, iL_y\psi_i^{g(u)}). \tag{3}$$

Taking the initial values as $a_1^+(-\infty) = 1$, $a_1^-(-\infty) = 0$ and $a_j^{+(-)}(-\infty) = 0$ for j greater than one, the coefficients $a_j^+(a_j^-)$ describe the direct (exchange) scattering processes.

The centre-of-mass differential cross sections are given in the impact-parameter approximation by (McCarroll and Salin 1968)

$$\sigma_i^{+(-)}(\theta) = 2\pi\mu^2 v^2 \left|\int_0^\infty db\, bT_i^{+(-)}(b)J_m(2\mu vb\sin\tfrac{1}{2}\theta)\right|^2 \tag{4}$$

where μ, v, θ and b are the reduced mass, the initial velocity, scattering angle and impact parameter respectively; the order m of the Bessel function is the difference between the magnetic quantum numbers in the initial and final states. Finally, the impact-parameter amplitude $T_j^{+(-)}$ is given by

$$T_j^{+(-)}(b) = a_j^{+(-)}(\infty) \exp\left(-\frac{\mathrm{i}}{2} \int_{-\infty}^{+\infty} [\epsilon_j^{\mathrm{g}} - \epsilon_j^{\mathrm{g}}(\infty) + \epsilon_j^{\mathrm{u}} - \epsilon_j^{\mathrm{u}}(\infty)] \, \mathrm{d}t \right) - \delta \tag{5}$$

where $\delta = 1$ for elastic transitions out of the initial state and zero otherwise. Integral cross sections are easily obtained from

$$Q_j^{+(-)}(E) = 2\pi \int_0^{\infty} \mathrm{d}b \, b \, |T_j^{+(-)}(b)|^2. \tag{6}$$

3. Results and discussion

3.1. Differential cross sections

It is well known from previous calculations that the major non-adiabatic process in proton–hydrogen scattering is the $1s$–$2p_{\pm 1}$ excitation due to the rotational coupling $2p\sigma_u \rightarrow 2p\pi_u$ at small internuclear distances (Bates and Williams 1964, McCarroll and Piacentini 1970, Chidichimo-Frank and Piacentini 1974, Gaussorgues *et al* 1975). Chidichimo-Frank and Piacentini (1974) and Rosenthal (1971) enlarged the expansion basis and found that the states $3p\sigma_u$ and $3p\pi_u$ do not affect the elastic, the resonance charge-exchange and the $2p_{\pm 1}$ excitation cross sections significantly, since the coupling of these states with the $2p\sigma_u$ and $2p\pi_u$ states respectively is relatively weak compared with the dominant $2p\sigma_u$–$2p\pi_u$ coupling. But the 2s, $2p_0$ and $3p_{\pm 1}$ excitation processes might be very sensitive to the inclusion of different states. In order to study this prediction, we used four expansion sets, listed in table 1, to calculate differential cross sections.

The states $2s\sigma_g$, $3d\sigma_g$ and the corresponding ungerade states tend to linear combinations of 2s and $2p_0$ hydrogen orbitals as R goes to infinity (Hatton *et al* 1975). Therefore we have to consider linear combinations $|2s\sigma_g\rangle \pm |3d\sigma_g\rangle$ and $|3p\sigma_u\rangle \pm |4f\sigma_u\rangle$ to calculate $\sigma_{2s}^{+(-)}$ and $\sigma_{2p_0}^{+(-)}$ respectively. However, the numerical calculations show that the probability for $3d\sigma_g$ and $4f\sigma_u$ excitation is very small; therefore $\sigma_{2s}^{+(-)}$ and $\sigma_{2p_0}^{+(-)}$ nearly coincide, as was pointed out by Chidichimo-Frank and Piacentini (1974).

It should be noted that we only considered the rotational coupling between the Σ and Π states. The radial coupling elements lead to spurious long-range coupling if energy-dependent translational factors are not included in the expansion (1) (Bates and Sprevak 1971). But we believe that this omission is justified for proton–hydrogen scattering, because the radial coupling elements are much smaller than the rotational coupling elements (Schinke and Krüger 1976).

We show in figure 1 the elastic, total charge-exchange and $2p_{\pm 1}$ excitation cross sections σ_{1s}^{+}, $\sigma^{-} = \Sigma_j \sigma_j^{-}$ and $\sigma_{2p_{\pm 1}}^{+}$ respectively for $E_{\mathrm{lab}} = 250$, 700 and 2000 eV calculated with expansion I and both straight-line and Coulomb trajectories. The agreement between our theoretical results and the experimental data is excellent even for higher energies. The more realistic Coulomb trajectories affect the cross sections

Table 1. Molecular basis sets used to calculate the differential cross sections.

Notation	Number of states	Molecular states		Asymptotic hydrogen states
I	4	$\|1s\sigma_g\rangle$	$\|2p\sigma_u\rangle$	$\|1s\rangle$
		$\|3d\pi_g\rangle$	$\|2p\pi_u\rangle$	$\|2p_{\pm1}\rangle$
II	10	$\|1s\sigma_g\rangle$	$\|2p\sigma_u\rangle$	$\|1s\rangle$
		$\|3d\pi_g\rangle$	$\|2p\pi_u\rangle$	$\|2p_{\pm1}\rangle$
		$\|4d\pi_g\rangle$	$\|3p\pi_u\rangle$	$\|3p_{\pm1}\rangle$
		$\|2s\sigma_g\rangle$	$\|3p\sigma_u\rangle$	$\frac{1}{\sqrt{2}}(\|2s\rangle + \|2p_0\rangle)$
		$\|3d\sigma_g\rangle$	$\|4f\sigma_u\rangle$	$\frac{1}{\sqrt{2}}(\|2s\rangle - \|2p_0\rangle)$
III	6	$\|1s\sigma_g\rangle$	$\|2p\sigma_u\rangle$	$\|1s\rangle$
		$\|3d\pi_g\rangle$	$\|2p\pi_u\rangle$	$\|2p_{\pm1}\rangle$
		$\|4d\pi_g\rangle$	$\|3p\pi_u\rangle$	$\|3p_{\pm1}\rangle$
IV	8	$\|1s\sigma_g\rangle$	$\|2p\sigma_u\rangle$	$\|1s\rangle$
		$\|3d\pi_g\rangle$	$\|2p\pi_u\rangle$	$\|2p_{\pm1}\rangle$
		$\|2s\sigma_g\rangle$	$\|3p\sigma_u\rangle$	$\frac{1}{\sqrt{2}}(\|2s\rangle + \|2p_0\rangle)$
		$\|3d\sigma_g\rangle$	$\|4f\sigma_u\rangle$	$\frac{1}{\sqrt{2}}(\|2s\rangle - \|2p_0\rangle)$

at larger angles in the same way as shown earlier by Gaussorgues *et al* (1975), although their 'common trajectory' method is somewhat different from the impact-parameter approximation adopted in this work.

The direct cross sections $\sigma^+_{2s} = \sigma^+_{2p_0}$ and $\sigma^+_{3p_{\pm1}}$ are also plotted in figure 1; these are calculated in the ten-state expansion II with straight-line and Coulomb trajectories. They are about one order of magnitude smaller than $\sigma^+_{2p_{\pm1}}$, and the influence

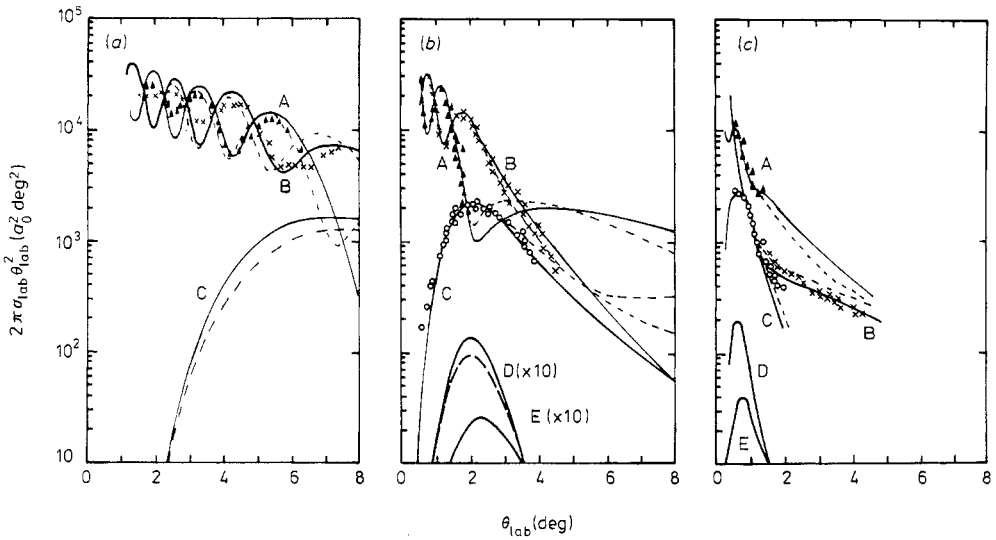

Figure 1. Reduced differential cross section $2\pi\sigma_{lab}\theta^2_{lab}$ plotted against the laboratory scattering angle θ_{lab} for E_{lab} = 250 eV (*a*), 700 eV (*b*) and 2000 eV (*c*). A(▲), direct elastic cross section σ^+_{1s}; B(×), total charge-exchange cross section $\sigma^- = \Sigma_i \sigma^-_i$; C(○) direct $2p_{\pm1}$ excitation cross section $\sigma^+_{2p_{\pm1}}$; D, 2s + $2p_0$ excitation cross section $\sigma^+_{2s} + \sigma^+_{2p_0}$; E, $3p_{\pm1}$ excitation cross section $\sigma^+_{3p_{\pm1}}$. A, B and C have been calculated with expansion I. D and E have been calculated with expansion II. Experimental data (▲, ×, ○) from Houver *et al* (1974). Full curves, straight-line trajectories; broken curves, Coulomb trajectories.

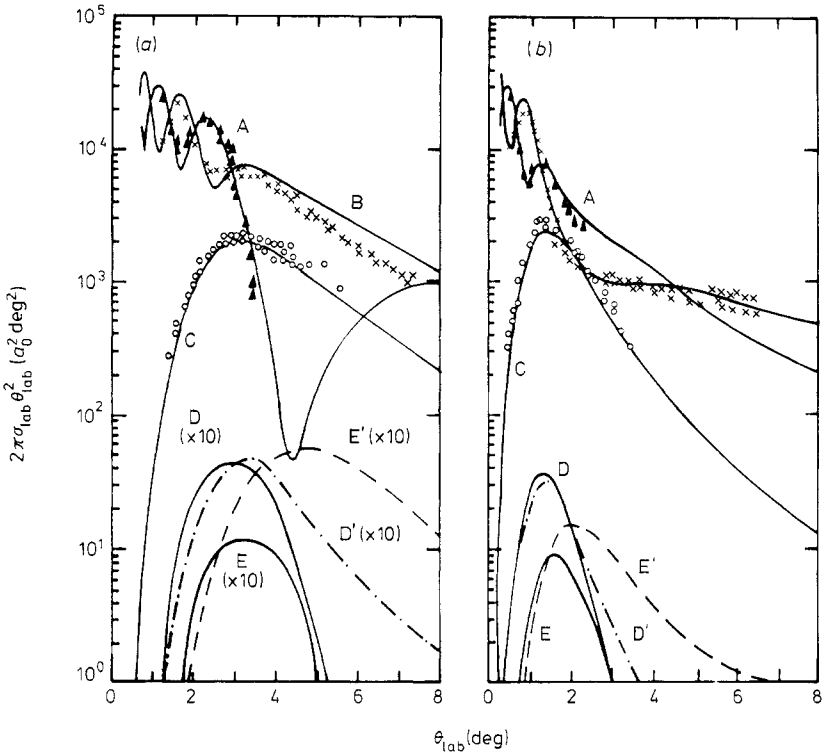

Figure 2. Reduced differential cross sections $2\pi\sigma_{lab}\theta_{lab}^2$ plotted against the laboratory scattering angle θ_{lab} for E_{lab} = 500 eV (*a*) and 1000 eV (*b*). A(▲), direct elastic cross section σ_{1s}^+; B(×), total charge-exchange cross section $\sigma^- = \Sigma_i\sigma_i^-$; C(○), direct $2p_{\pm1}$ excitation cross section $\sigma_{2p_{\pm1}}^+$; D, 2s + $2p_0$ excitation cross section $\sigma_{2s}^+ + \sigma_{2p_0}^+$; E, $3p_{\pm1}$ excitation cross section $\sigma_{3p_{\pm1}}^+$. A, B and C have been calculated with expansions I and II, D(D') and E(E') have been calculated with expansions II (IV) and II (III) respectively. Experimental data (▲, ×, ○) of Houver *et al* (1974); straight-line trajectories have been used throughout.

of the Coulomb trajectories is not so strong as for the other cross sections. Thus for E_{lab} = 2000 eV both results nearly coincide. While the maximum value of the reduced $2p_{\pm1}$ excitation cross section is only slightly energy-dependent, the converse is true for $\sigma_{2s}^{+(-)} = \sigma_{2p_0}^{+(-)}$ and $\sigma_{3p_{\pm1}}^{+(-)}$ in the energy range considered. This effect is also displayed in figure 2, where we study the influence of the different expansion sets on the reported cross sections for intermediate energies E_{lab} = 500 and 1000 eV. The elastic, charge-exchange and $2p_{\pm1}$ excitation cross sections are calculated with expansions I and II and straight lines, but the differences are too small to be depicted in the figure. The cross sections $\sigma_{2p_0}^+ = \sigma_{2s}^+$ are calculated in the ten (II) and the eight (IV) state expansions, where the states $4d\pi_g$ and $3p\pi_u$ have been omitted; accordingly $\sigma_{3p_{\pm1}}^+$ is calculated with expansions II and III. From figure 2 we clearly see that these cross sections are strongly affected by different expansions. The reason for this behaviour is that the magnitudes of $\sigma_{2s}^{+(-)} = \sigma_{2p_0}^{+(-)}$ and $\sigma_{3p_{\pm1}}^{+(-)}$ are comparable. Thus the omission of one excitation process enhances the other.

Another point worthy of mention is that the excited gerade states have no influence on the cross sections in the energy range considered. This holds for both

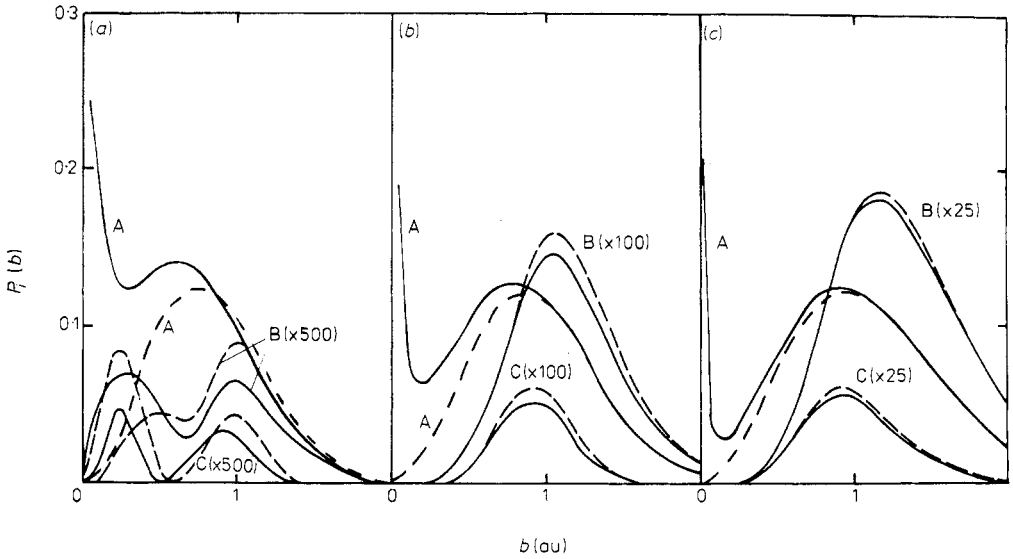

Figure 3. Direct transition probabilities $P_i^+ = |T_i^+|^2$ plotted against the impact parameter b for $E_{lab} = 0{\cdot}5$ keV (*a*), 1 keV (*b*) and 2 keV (*c*). A, $2p_{\pm 1}$ excitation probability; B, $2s + 2p_0$ excitation probability; C, $3p_{\pm 1}$ excitation probability. Full curves, Coulomb trajectories; broken curves, straight-line trajectories. A has been calculated with expansion I, B and C have been calculated with expansion II.

the elastic and resonance charge-transfer cross sections as well as for all excitation cross sections. A consequence of this finding is that the excitation cross sections for direct and exchange processes nearly coincide (see e.g. Chidichimo-Frank and Piacentini 1974, figure 1).

In figure 3 we show the probabilities $P_i^{+(-)}(b) = |T_i^{+(-)}(b)|^2$ for the direct excitation processes calculated with straight-line and Coulomb trajectories. First we note that some of the statements made for cross sections also hold for the probabilities. While the Coulomb trajectories produce a narrow maximum at small impact parameters in $P_{2p_{\pm 1}}^+$, they do not affect the probabilities for the 2s, $2p_0$ and $3p_{\pm 1}$ excitations significantly. On the other hand $P_{2s}^+ = P_{2p_0}^+$ and $P_{3p_{\pm 1}}^+$ show a second peak even for the straight-line trajectories for energies $E_{lab} < 700$ eV. This has also been observed by Gaussorgues and Salin (1971) who employed an atomic expansion of the electronic wavefunction.

A more unbiased comparison between theory and experiment is afforded by the total exchange probability

$$P_{ex}(\theta) = \frac{\sigma^-(\theta)}{\Sigma_i(\sigma_i^+(\theta) + \sigma_i^-(\theta))}. \tag{7}$$

The corresponding results for $E_{lab} = 250$, 700 and 1000 eV together with the experimental data of Helbig and Everhart (1965) and Houver *et al* (1974) are presented in figure 4. In figure 5 we compare the fractional charge-exchange probability to the 2s hydrogen state

$$P_{ex}'^{2s} = \frac{\sigma_{2s}^-(\theta)}{\Sigma_i \sigma_i^-(\theta)} \tag{8}$$

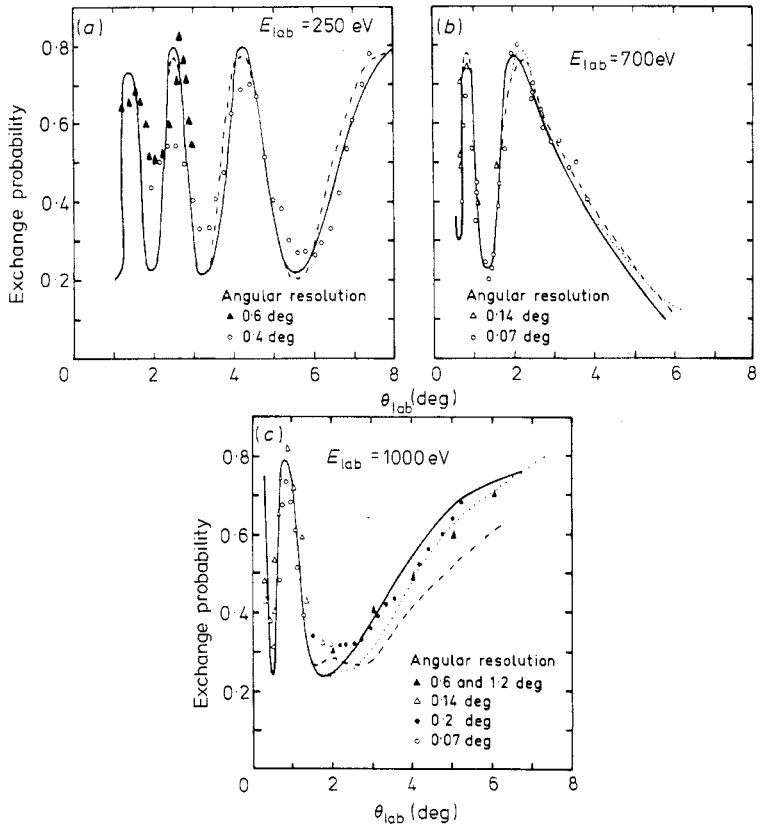

Figure 4. Charge-exchange probability $P_{ex}(\theta_{lab})$ plotted against the laboratory scattering angle θ_{lab} for $E_{lab} = 250$ eV (*a*), 700 eV (*b*) and 1000 eV (*c*). Experimental data: ▲, △, Helbig and Everhart (1965); ●, ○, Houver *et al* (1974). Theoretical results: ——, present calculations using the four-state expansion (I) and straight-line trajectories; – – –, McCarroll and Piacentini (1970); · · · ·, Gaussorguez *et al* (1975). Angular resolutions: (*a*) ▲, 0·6°; ○, 0·4°; (*b*) △, 0·14°; ○, 0·07°; (*c*) ▲, 0·6° and 1·2°; △, 0·14°; ●, 0·2°; ○, 0·07°.

with the measured data of Bayfield (1970) and the theoretical results of Chidichimo-Frank and Piacentini (1974) for $E_{lab} = 6$ keV.

Some of the characteristic features of the differential cross sections can be explained qualitatively in terms of the united-atom limit of the angular momentum matrix elements (Rosenthal 1971):

$$\langle nlm|iL_y|n'l'm'\rangle = [\tfrac{1}{2}l(l+1)]^{1/2}\delta_{ll'}\delta_{nn'}\delta_{mm'\pm 1} \tag{9}$$

where n, l, m are the principal, the angular momentum and the magnetic quantum numbers in that limit. Chidichimo-Frank and Piacentini (1974) stated that the region of small internuclear distances plays a fundamental role in this collision process. From (9) we easily see that the coupling between two states can be strong only if they tend to the same united-atom limit, and if their magnetic quantum numbers differ by ± 1. Accordingly, the coupling schemes for ungerade and gerade states are shown in figure 6 where strong ($\Rightarrow$) and weak ($\longrightarrow$) couplings are exhibited. From figure 6 it can be seen that the gerade states play an unimportant role, because the first coupling steps $1s\sigma_g \longrightarrow 3d\pi_g$ and $1s\sigma_g \longrightarrow 4d\pi_g$ are very weak compared with

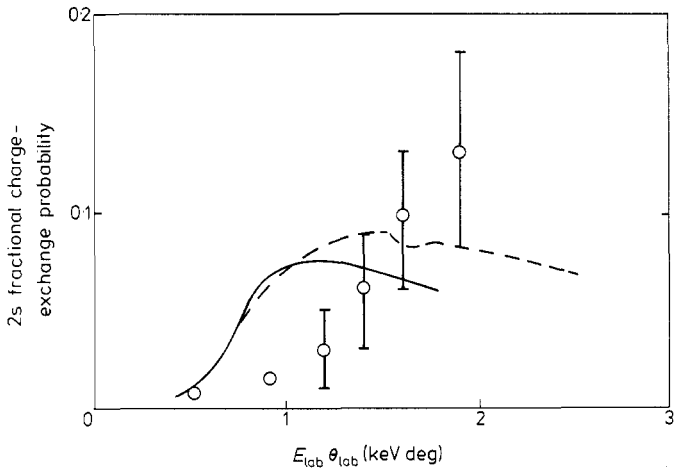

Figure 5. Fractional charge-exchange probability of the 2s state of hydrogen plotted against the product of impact energy (6 keV) and the laboratory scattering angle θ_{lab}. Full curve, present results calculated in the ten-state expansion (II) using straight-line trajectories; broken curve, results of Chidichimo-Frank and Piacentini (1974) calculated in a five-state expansion. Experimental data of Bayfield (1970).

the $2p\sigma_u \rightarrow 2p\pi_u$ coupling. In addition, it is obvious that the $2p_{\pm 1}$ excitation is the most important non-adiabatic effect, because the $2p_0$ and 2s excitations are caused by two-step coupling processes and the $2p\sigma_u \rightarrow 3p\pi_u$ coupling which gives rise to the $3p_{\pm 1}$ excitation is quite weak.

3.2. *Integral cross sections*

We calculated integral cross sections $Q_i^{+(-)}(E)$ for inelastic, direct and exchange processes in the energy range $1\,\text{keV} \leqslant E_{lab} \leqslant 10\,\text{keV}$ applying the ten-state expansion II and Coulomb trajectories. The results for $Q^-_{2p_{\pm 1}}$, $Q^-_{2s} = Q^-_{2p_0}$ and $Q^-_{3p_{\pm 1}}$ are plotted in figure 7 and compared with the experimental data of Morgan *et al* (1973). The agreement is quite good for smaller energies but decreases with increasing collision

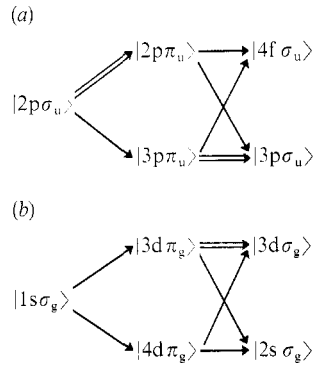

Figure 6. Rotational coupling schemes for (*a*) ungerade states and (*b*) gerade states. Strong (weak) coupling is indicated by $\Rightarrow(\rightarrow)$ according to the united-atom limit expression (9) for the angular momentum matrix elements.

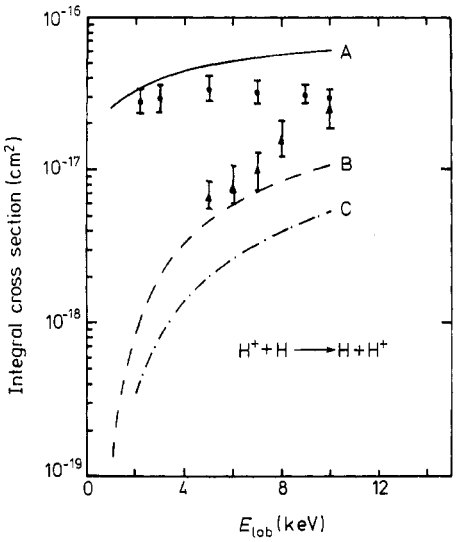

Figure 7. Exchange integral cross sections $Q_j^-(E_{lab})$ plotted against the impact energy E_{lab}. A, the $2p_{\pm1}$ excitation cross section $Q^-_{2p_{\pm1}}$; B, the 2s excitation cross section Q^-_{2s}; C, the $3p_{\pm1}$ excitation cross section $Q^-_{3p_{\pm1}}$. The experimental data are taken from Morgan *et al* (1973): ●, $2p_{\pm1}$ excitation exchange cross sections; ▲, 2s excitation exchange cross sections.

energies as one would expect from the use of an adiabatic expansion. As pointed out earlier for differential cross sections $\sigma_i^{+(-)}$ and probabilities $P_i^{+(-)}(b)$, the integral cross sections for 2s, $2p_0$ and $3p_{\pm1}$ excitation increase more rapidly as a function of energy than the $2p_{\pm1}$ excitation cross section. The theoretical cross sections for the equivalent direct processes are very similar to those shown in figure 7, although the experimental direct and exchange cross sections are quite different (see figures 8 and 9 of Morgan *et al* 1973). This result is a consequence of the fact that the gerade states can be neglected in the molecular expansion. For $E_{lab} = 10\,keV$ the ratio $Q^+_{2p_{\pm1}}/Q^-_{2p_{\pm1}}$ is about 0·98 only.

4. Conclusions

We have calculated differential cross sections for direct and exchange processes in the energy range $0{\cdot}25\,keV \leqslant E_{lab} \leqslant 2\,keV$ using both straight-line and Coulomb trajectories within the impact-parameter method. The agreement between our theoretical results and the experimental elastic, charge-exchange and $2p_{\pm1}$ excitation cross sections is very good even at higher energies and larger scattering angles. The change from straight-line to Coulomb trajectories affects the cross sections at larger scattering angles and lower energies. The inclusion of higher excited states into the molecular expansion basis does not change the elastic, charge-exchange and $2p_{\pm1}$ excitation cross sections, but affects the cross sections for the 2s, $2p_0$ and $3p_{\pm1}$ excitation very significantly. Accordingly the $2s = 2p_0$ and $3p_{\pm1}$ excitation cross sections are small compared with the dominant $2p_{\pm1}$ excitation. The gerade states can be neglected in the energy range considered. A consequence of this is the fact that the cross sections for inelastic direct and exchange processes coincide. All of these results can be

explained qualitatively in terms of the rotational coupling scheme for the ungerade and gerade states and making use of the united-atom limit of the angular momentum matrix elements.

Acknowledgments

The authors are grateful for the financial support of the Deutsche Forschungsgemeinschaft.

References

Bates D R and Sprevak D 1971 *J. Phys. B: Atom. Molec. Phys.* **4** L47–51
Bates D R and Williams D A 1964 *Proc. Phys. Soc.* **83** 425–33
Bayfield J E 1970 *Phys. Rev. Lett.* **25** 1–3
Chidichimo-Frank M C and Piacentini R D 1974 *J. Phys. B: Atom. Molec. Phys.* **5** 548–57
Gaussorgues C, Le Sech C, Masnou-Seeuws F, McCarroll R and Riera A 1975 *J. Phys. B: Atom. Molec. Phys.* **8** 253–64
Gaussorgues C and Salin A 1971 *J. Phys. B: Atom. Molec. Phys.* **4** 503–12
Hatton J H, Chen J C Y and Ishihara T 1975 *Phys. Rev.* A **12** 1281–95
Helbig H F and Everhart E 1965 *Phys. Rev.* **140** A715–20
Houver J C, Fayeton J and Barat M 1974 *J. Phys. B: Atom. Molec. Phys.* **7** 1358–69
McCarroll R and Piacentini R D 1970 *J. Phys. B: Atom. Molec. Phys.* **3** 1336–45
McCarroll R and Salin A 1968 *J. Phys. B: Atom. Molec. Phys.* **2** 163–71
Morgan T J, Geddes J and Gilbody H B 1973 *J. Phys. B: Atom. Molec. Phys.* **6** 2118–38
Rosenthal H 1971 *Phys. Rev. Lett.* **27** 635–8
Schinke R and Krüger H 1976 *J. Chem. Phys.* **64** 2450